AD-A087 118 DUMONT ELECTRON TUBES CLIFTON N J F/G 3/2
COROTATION OF SATURN'S MAGNETOSPHERE: EVIDENCE FROM ENERGETIC P--ETC(U)
JUN 80 M F THOMSEN, T G NORTHROP, A W SCHARDT N00014-76-C-0016
UNCLASSIFIED U. OF IOWA-80-14 NL

1 of 1
AD A 087 118

END
DATE FILMED
9-80
DTIC

U. of Iowa 80-

LEVEL II

12

AD A087118

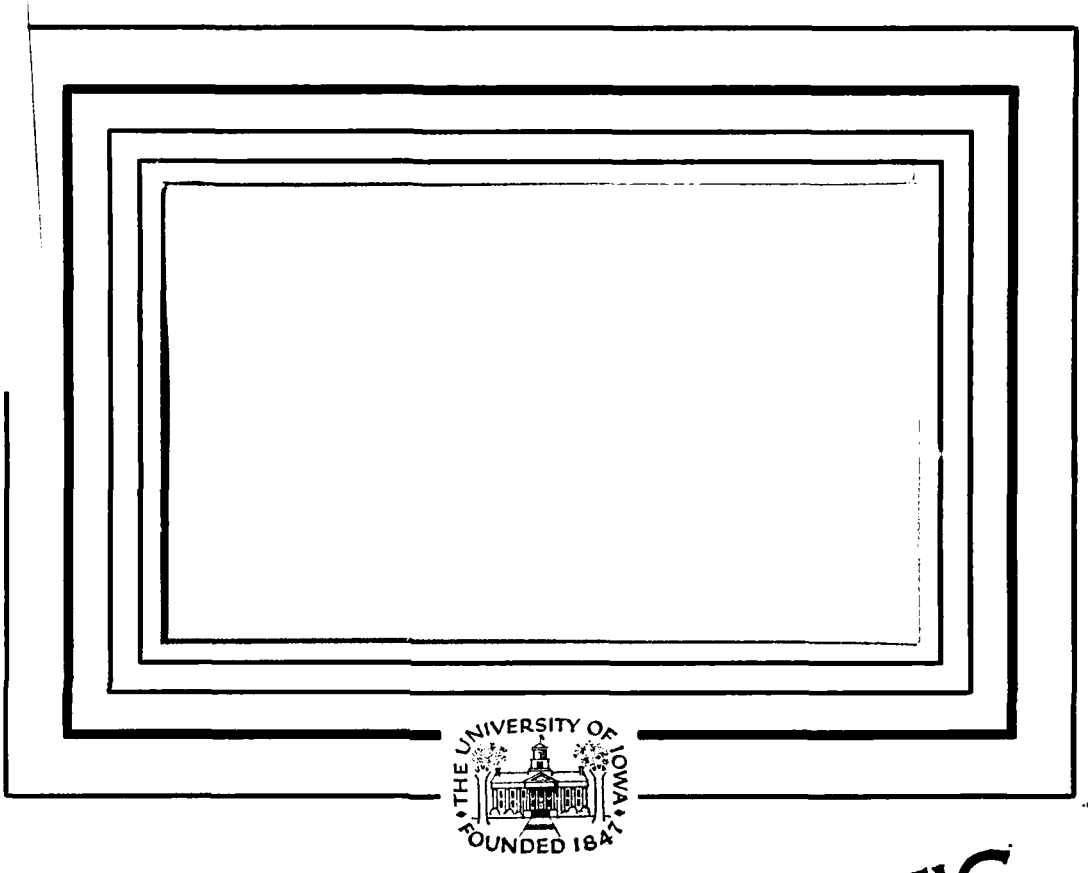

DTIC
SELECTE
JUL 24 1980
S D
C

Department of Physics and Astronomy

THE UNIVERSITY OF IOWA

Iowa City, Iowa 52242

80 7 23 02

U. of Iowa 80-14

12

Corotation of Saturn's Magnetosphere: Evidence from Energetic Proton Anisotropies

by

M. F. THOMSEN,* T. G. NORTHROP,† A. W. SCHARDT,†

and J. A. VAN ALLEN*

Department of Physics and Astronomy
The University of Iowa
Iowa City, Iowa 52242

June 1980

*Department of Physics and Astronomy, University of Iowa, Iowa City, Iowa 52242.

†NASA/Goddard Space Flight Center, Greenbelt, Maryland 20771.

Revised version of original manuscript of 28 April 1980.

In press, J. Geophys. Res.

UNCLASSIFIED

SECURITY CLASSIFICATION OF THIS PAGE (When Data Entered)

REPORT DOCUMENTATION PAGE	READ INSTRUCTIONS BEFORE COMPLETING FORM
1. REPORT NUMBER: U. of Iowa-80-14 (14)	2. GOVT ACCESSION NO.: AD-A087118
3. RECIPIENT'S CATALOG NUMBER: --	
4. TITLE (and Subtitle): COROTATION OF SATURN'S MAGNETOSPHERE: EVIDENCE FROM ENERGETIC PROTON ANISOTROPIES. Revision. (6)	5. TYPE OF REPORT & PERIOD COVERED: Progress rept. June 1980 (9)
	6. PERFORMING ORG. REPORT NUMBER: -- (15)
7. AUTHOR(s): M. F. Thomsen, T. G. Northrop, A. W. Schardt, J. A. Van Allen (10)	8. CONTRACT OR GRANT NUMBER(s): N00014-76-C-0016, NAS2-6553
9. PERFORMING ORGANIZATION NAME AND ADDRESS: Department of Physics and Astronomy, The University of Iowa, Iowa City, Iowa 52242	10. PROGRAM ELEMENT, PROJECT, TASK AREA & WORK UNIT NUMBERS: --
11. CONTROLLING OFFICE NAME AND ADDRESS: Office of Naval Research, Electronics Program Office, Arlington, Virginia 22217	12. REPORT DATE: June 1980 (11)
	13. NUMBER OF PAGES: 33
14. MONITORING AGENCY NAME & ADDRESS (if different from Controlling Office): (12) 35	15. SECURITY CLASS. (of this report): UNCLASSIFIED
	15a. DECLASSIFICATION/DOWNGRADING SCHEDULE

16. DISTRIBUTION STATEMENT (of this Report)

Approved for public release; distribution is unlimited.

17. DISTRIBUTION STATEMENT (of the abstract entered in Block 20, if different from Report)

18. SUPPLEMENTARY NOTES

To be published in J. Geophys. Res.

19. KEY WORDS (Continue on reverse side if necessary and identify by block number)

Saturn's magnetosphere
Corotation

20. ABSTRACT (Continue on reverse side if necessary and identify by block number)

[See page following.]

DD FORM 1 JAN 73 1473 EDITION OF 1 NOV 65 IS OBSOLETE
S/N 0102-LF-014-6601

UNCLASSIFIED
SECURITY CLASSIFICATION OF THIS PAGE (When Data Entered)

ABSTRACT

The theory and technique of Northrop and Thomsen [1980] are applied to observations of energy spectra and directional anisotropies of 0.61 - 3.41 MeV protons in Saturn's magnetosphere. The observations were made by the Goddard Space Flight Center/University of New Hampshire and University of Iowa instruments aboard Pioneer 11 during the Pioneer encounter with Saturn in August/September 1979. Fourier fits to 15-minute intervals of data are combined with spectral indices to yield information about the $\vec{E} \times \vec{B}$ convection velocity and temporal changes in the particle population. There is a fundamental inability to distinguish unambiguously between the two, but if one can be assumed, the other then follows from these calculations. It is found that although these data do not by themselves allow an unambiguous determination of the extent of corotation in Saturn's outer magnetosphere, they are consistent with exact corotation at the nominal rotation period in the presence of significant but not unreasonable temporal variations in the energetic proton population.

Introduction

In magnetospheric physics, the extent to which a planet's ionosphere is electrically coupled to its magnetosphere is of considerable interest. A measure of this coupling is the degree to which the charged particles in the magnetosphere corotate with the planet. One thus would like to be able to measure the $\vec{E} \times \vec{B}$ convection velocity of magnetospheric particles and compare it with the corotational velocity.

In an accompanying paper, Northrop and Thomsen [1980] outline the theory and technique by which spacecraft observations of angular distributions and energy spectra of energetic particles may be used to deduce $\vec{E} \times \vec{B}$ flow velocities under certain circumstances. In this paper, we apply the results of Northrop and Thomsen to observations of energetic protons in Saturn's magnetosphere obtained by the University of Iowa and Goddard Space Flight Center/University of New Hampshire instruments aboard Pioneer 11.

Figure 1, from Van Allen et al. [1980a] shows the equatorial plane projection of the encounter trajectory of Pioneer 11. The plane of the Pioneer orbit was inclined by 6.6° relative to Saturn's equatorial plane. The spacecraft spin axis points continuously at the Earth, and both the Iowa and GSFC/UNH instruments have their view direction perpendicular to the spacecraft spin axis so that as the spacecraft spins, the detectors scan the particle distribution in a plane perpendicular to the spin axis. From Figure 1 it can be

seen that on the inbound portion of the encounter trajectory, the spacecraft spin axis was roughly in the radial direction relative to Saturn. The Iowa and GSFC/UNH instruments thus scanned in a plane nearly perpendicular to the radial direction and were therefore favorably arranged to observe anisotropies associated with corotational motion. On the outbound portion of the trajectory, the detectors essentially scanned in a meridian plane, and therefore azimuthal flow would not have been seen. In this paper we report observations made on the inbound portion of the trajectory between about 15 and 6 R_S.

Instrumentation

The University of Iowa experiment on Pioneer 11 is described elsewhere in this issue [Van Allen et al., 1980b]. In this paper we are concerned with observations obtained by detector G, which is a thin solid-state detector sensitive to protons in the energy range 0.61 to 3.41 MeV. As discussed by Van Allen et al. [1980b], detector G is a directional detector with a measured angular response function having FWHM = 36°. At the bit rate and telemetry format prevailing during the Saturn encounter, detector G was sampled twice every 8.25 seconds, each sample representing an accumulation period of 0.75 seconds. The spacecraft spin period during encounter was 7.693 sec, so each detector readout represented a scan through 35.1 degrees. Each sample was labelled according to the spacecraft roll angle of the detector axis at the center of the accumulation period. (The roll angle is the angle measured in the scan plane from the ascending node of the scan plane on the ecliptic.)

Both the finite angular response of the detector and the finite sampling time have the effect of "smearing out" the observed angular distribution. That is, if the true angular distribution can be represented by a Fourier expansion of the form

$$R(\varphi) = M\left[1 + \sum_{i=1}^{\infty} K_i \cos i(\varphi - \Delta_i)\right] \quad , \qquad (1)$$

then a Fourier analysis of the detector counting rate would yield smaller values for the Fourier coefficients than the true K_i in the actual distribution. This reduction factor can be calculated for each Fourier coefficient, and the observed values can thus be corrected for the smear effect. The correction factors for the Fourier coefficients K_1, K_2, K_3 are 1.039, 1.160, and 1.402, respectively.

The University of Iowa detector G provides good angular resolution but no spectral information. The GSFC/UNH instrument [Trainor et al., 1974] provides detailed energy spectra ($0.2 < E_p < 20$ MeV) spanning the energy window of the Iowa detector. The GSFC/UNH experiment also measures angular distributions which agree closely with the Iowa observations. Since the GSFC/UNH experiment is primarily designed for cosmic ray observations, its telemetry assignment during encounter was minimal. Therefore, this part of the GSFC/UNH data could not significantly improve the overall statistical accuracy and was not used. The two experiments thus provide complementary information, and we combine the spectral information available from the Goddard system with the angular distributions obtained by the Iowa detector to obtain the results to be presented below.

Observations

Counting rates from the University of Iowa detector G have been fit in 15-minute intervals to a function of the form of Equation (1), with i = 1,2,3. The fitting procedure was a linear least-squares approach rather than a true Fourier analysis, but for the nearly uniform roll angle coverage represented by 15 minutes worth of data, the two procedures are equivalent. Figure 2 shows the results of the fit for data acquired inbound between about 15 and 5 R_S. Note that there is a significant first order anisotropy whose amplitude (K_1) tends generally to decrease with decreasing distance from Saturn and whose phase (Δ_1) is more or less persistently parallel to the equatorial plane (i.e., $\Delta_1 \sim 153°$) in the direction appropriate for corotation. Such a first order anisotropy is qualitatively consistent with a Compton-Getting effect due to corotation. Note also the strong second order anisotropy whose phase (Δ_2) is also approximately parallel to the equatorial plane, indicating that these are "pancake" distributions, i.e., peaked near a pitch angle of 90°. A pancake distribution is the normal signature of a durably trapped particle population. Figure 3 shows sample comparisons between the data and corresponding fits for two of the 15-minute intervals.

The Fourier coefficients K_1, K_2, and K_3 shown in Figure 2 were subsequently corrected for the smear due to finite detector geometry and sampling time as discussed above. The corrected values

are related to the Fourier coefficients (A_o, A_1, A_2, A_3) of Northrop and Thomsen [1980] by

$$M = A_o$$
$$K = A_i/A_o \quad i = 1,2,3 \quad . \tag{2}$$

The phase angles Δ_i $(i = 1,2,3)$ shown in Figure 2 are related to the phase angles χ_i of Northrop and Thomsen [1980] by

$$\Delta_i = \chi_i + \varphi_B \tag{3}$$

where φ_B is the roll angle of the projection of the magnetic field vector on to the scan plane of the detector (i.e., on to the spacecraft equatorial plane). φ_B is thus the roll angle of the $\hat{p}$ vector in the notation of Northrop and Thomsen, and their angle χ is just $\chi = \varphi - \varphi_B$.

With the notation changes discussed above, the corrected Fourier coefficients and phase angles can be directly substituted into Equations (24) and (25) of Northrop and Thomsen [1980], which relate the convection velocity $\vec{u}_E$ to the spatial gradient of the intensity of particles having an energy within the window of the detector. For ease in application, Equations (24) and (25) can be combined to show the dependence on each Fourier coefficient, i.e.,

$$\frac{2\gamma - 3}{\gamma - 1/2}(\gamma + 1 - K_2)\frac{1 - R^{\gamma-1/2}}{1 - R^{\gamma-3/2}}\frac{\vec{u}_E}{v_1}$$

$$+ \frac{v_1}{\omega}\frac{\hat{e}_1 \times \nabla M}{M} = K_1\vec{\eta}_1 + K_2\vec{\eta}_2 + K_3\vec{\eta}_3 \qquad (4)$$

where γ is the differential spectral index and

$$\vec{\eta}_1 = \left(\frac{\gamma - 3/2}{\gamma - 1}\right)\left(\frac{1 - R^{\gamma-1}}{1 - R^{\gamma-3/2}}\right)\left[-\hat{n}_1 + \frac{1}{\sin i}(\hat{e}_1 \cdot \hat{n}_1)\hat{z}\right]$$

$$\vec{\eta}_2 = \frac{2v_1}{\omega}\hat{e}_1 \times \frac{\partial \hat{e}_1}{\partial s} - \frac{v_1}{\omega}\left(\tan i\ \hat{q}\hat{q} + \frac{1}{2}\hat{p}\hat{z} - \frac{1}{2}\cot i\ \hat{z}\hat{z}\right) \cdot \hat{e}_1$$

$$\times\left[\cot i \frac{\partial \hat{e}_1}{\partial s} + \hat{e}_1 \times \frac{\partial \hat{e}_1}{\partial q} - \frac{1}{\sin i}\frac{\partial \hat{e}_1}{\partial p}\right]$$

$$\vec{\eta}_3 = \left(\frac{\gamma - 3/2}{\gamma - 1}\right)\left(\frac{1 - R^{\gamma-1}}{1 - R^{\gamma-3/2}}\right)\left[-\hat{n}_3 \cdot \left(\hat{q}\hat{q} - \hat{p}\hat{p} + \cot i\ \hat{p}\hat{z}\right)\right] \quad .$$

The parameters and vectors used in Equation (4) are defined in Northrop and Thomsen [1980]. For the present study, the unit vector $\hat{e}_1$ in the direction of the magnetic field (and its angle of inclination to the scan plane, i) was obtained from the observed magnetic field data [courtesy E. J. Smith et al.]. However, the components of the gradient of $\hat{e}_1$ (i.e., $\partial\hat{e}_1/\partial s$, $\partial\hat{e}_1/\partial p$, and $\partial\hat{e}_1/\partial q$) were calculated assuming a dipole field model [see Equation (23) of Northrop and Thomsen]. The dipole approximation is applied because Smith

et al. [1980] have shown that during the Pioneer 11 encounter, the dayside magnetic field of Saturn was indeed quite dipolar in shape, rather than being flattened and distended by a large current sheet as is Jupiter's magnetosphere. For the University of Iowa detector G, the ratio R of lower to upper threshold energies is 0.179, and the velocity v_1 of protons with the lower threshold energy is 1.08×10^9 cm/sec. The local proton gyrofrequency ω was calculated from the observed magnetic field strength.

The final observational parameter required in Equation (4) is the differential spectral index γ. Equation (4) is based on the assumption that the energy spectrum is a strict power law. McDonald et al. [1980] have shown, however, that beyond about 11.5 R_S, the proton energy spectrum is better fit by a sum of two power laws. The left panel of Figure 4 shows an example of such a spectrum. We may nevertheless obtain an effective γ from such a spectrum for use in Equation (4) because the fact that the proton intensity decreases with increasing energy means that an integral detector is principally responding to particles with energies near the lower detector threshold. Thus the power law spectral index which applies in the neighborhood of the lower threshold energy can be used as an effective spectral index for our calculation. Inside of 11 R_S, the spectrum can be represented by a single power law, as shown in the right panel of Figure 4. Figure 5 shows the spectral index determined by the GSFC/UNH instrument during the inbound portion of the

encounter. Each point is located at the center of the 30-minute interval over which data were averaged to determine the spectrum. In the range within which the four-parameter spectrum provides a better fit to the data, the effective γ at the lower threshold of the University of Iowa detector G is shown. For the purpose of evaluating Equation (4), the values of γ appropriate to the time intervals for which anisotropy parameters were determined were obtained by linearly interpolating between the values plotted in Figure 5.

Results

In Equation (4) it can be seen that both an $\vec{E} \times \vec{B}$ ($= \vec{u}_E$) convection velocity and a spatial gradient of the density (∇M) perpendicular to the magnetic field will give rise to a first order anisotropy. For a spacecraft near the magnetic equatorial plane such as Pioneer 11 at Saturn, a radial density gradient results in an $\hat{e}_1 \times \nabla M$ contribution to the anisotropy which is in the azimuthal direction, i.e., the same direction as the anisotropy arising from a corotational $\vec{u}_E$. It can also be seen from Equation (4) that a second order anisotropy, in the presence of magnetic curvature or shear, will also contribute to a first order anisotropy. There will also be a small contribution from any third order anisotropy, but as shown in Figure 2, the third order anisotropy amplitude is generally quite low.

As Northrop and Thomsen [1980] have pointed out, the separate contributions of spatial gradients and $\vec{E} \times \vec{B}$ drifts to particle anisotropies can not be uniquely identified using Equation (4). If, however, one knows or can assume something about the spatial gradients, Equation (4) allows the calculation of $\vec{u}_E$. Conversely, if $\vec{u}_E$ is known, the gradient can be calculated. In the case of the Pioneer 11 encounter with Saturn, there are two different situations we may explore: One is a steady-state magnetosphere and the other is a corotating magnetosphere.

a. Steady State

If the magnetospheric configuration and particle distribution were unchanging during the encounter, then the changes in particle intensity observed by Pioneer 11 as it traversed the magnetosphere (see top panel of Figure 2) can be attributed to a spatial distribution alone. Since the spacecraft velocity is known, the gradient of M (at least the component of the gradient parallel to the spacecraft trajectory) can be estimated. Equation (4) then yields the convection velocity $\vec{u}_E$.

Figure 6 shows the azimuthal component of $\vec{u}_E$ which results from Equation (4) for a time-stationary situation. Since the spacecraft motion was predominantly radial, the variations in M seen in Figure 2 have been attributed to a purely radial gradient, with the nonradial components of the gradient assumed to be zero. As mentioned earlier, a radial intensity gradient should produce an anisotropy in the same direction as a corotational $\vec{u}_E$. The values of the azimuthal component of $\vec{u}_E$ plotted in Figure 6 have been smoothed with a four-point (i.e., one hour) running average to accentuate lower-frequency structure. Also shown in Figure 6 as a solid line is the azimuthal component of the convection velocity one would expect for particles exactly corotating with the nominal planetary rotation period at $10^h\ 40^m$ [Kaiser et al., 1980].

A weighted least-squares fit of the azimuthal velocity component to a function of the form $u_E = r\Omega$ gives

$$\Omega = [1.729\ (\pm\ 0.229)] \times 10^{-4}\ s^{-1}$$

which corresponds to a rotational period of

$$P = 10^h\ 6^m\ \begin{matrix} + 1^h\ 32^m \\ - 1^h\ 11^m \end{matrix} .$$

This rotation period gives the dashed line in Figure 6. Thus, although Figure 6 shows apparently significant deviations from exact corotation when a steady state is assumed, on the average the results are consistent with corotation at the nominal rate.

b. Exact Corotation

If the magnetosphere is corotating exactly, then $\vec{u}_E$ is known and Equation (4) yields the gradient of the particle intensity. This gradient, dotted with the spacecraft velocity, tells us the convective part of the time variations in the intensity observed by the spacecraft. Subtracting this from the total time derivative actually observed by the spacecraft leaves an estimate of the purely temporal changes in the intensity, i.e., $\partial(\log M)/\partial t$.

Figure 7 shows the values of $\partial(\log M)/\partial t$ which result from assuming exact corotation at the nominal period of $10^h\ 40^m$ (again smoothed with a four-point running average). There are intervals of time during which the partial time derivative is found to be significantly nonzero, but a weighted average over all the data shown in Figure 7 gives an average time change over the entire interval of

$$\left\langle \frac{\partial(\log M)}{\partial t} \right\rangle = [-\ 4.9\ (\pm\ 14.5)] \times 10^{-4}\ \text{min}^{-1} \quad .$$

The average temporal change when exact corotation is assumed is thus zero within the errors.

To test the sensitivity of this result, we have also computed $\partial(\log M)/\partial t$ for the case $\vec{u}_E = 0$. These results are shown in Figure 8. As can be seen from this figure, if zero corotation is assumed, the deduced partial time derivative is negative at almost all times. The average over the entire interval is

$$\left\langle \frac{\partial(\log M)}{\partial t} \right\rangle = [-\ 1.07\ (\pm\ 0.21)] \times 10^{-2}\ \text{min}^{-1} \quad ,$$

which would represent a net decrease in the energetic particle intensity by roughly a factor of 650 during this time period. Such a large decrease in the energetic particle content of the outer magnetosphere seems too large to be credible.

Discussion

As discussed in Northrop and Thomsen [1980], Equation (4) is derived on the basis of a model gyrotropic distribution function (f_o in their notation) which is pancake in shape, i.e., peaked near a pitch angle of 90°. This model is appropriate for the present study because, as shown in Figure 2, the energetic proton distribution was persistently pancake in nature ($\Delta_2 \sim 153°$) throughout Saturn's dayside magnetosphere. The model distribution function f_o also did not include a provision for parallel flow, but as can be seen in Figure 2, the exclusion of parallel flow from the treatment of anisotropies at Saturn appears to be valid since the first order anisotropy direction Δ_1 is always observed to be quite close to a direction perpendicular to the magnetic field. (A field-aligned flow would have $\Delta_1 \sim 63°$ or 243°.) This is in marked contrast to the situation during the Pioneer 10 encounter with Jupiter, where Northrop et al. [1979] found that the effects of parallel flow were very important and could not be excluded.

Figure 6 shows that on the average the convection velocity derived from Equation (4) when temporal changes are ignored is consistent with corotation at the nominal period. However, there are also times during which the apparent velocity would be significantly different from the corotation value. Of the 38 points shown in Figure 6, 22 (or 58%) of them deviate from the value

expected for exact corotation by more than 1σ, 3 (or 8%) lie at least 2σ away from exact corotation, and 1 (or 3%) lies at least 3σ away. For a normal distribution of errors, only 32%, 5%, and < 1% should lie more than 1σ, 2σ, and 3σ, respectively, away from the mean. A situation such as that near 11 R_S, where the deduced velocity is more than twice the value expected for exact corotation, would appear to be physically unrealistic, so the assumption of steady state is probably inappropriate during at least part of this period.

Large-scale temporal changes are not unreasonable in light of the highly disturbed solar wind conditions that were present during the Pioneer 11 Saturn encounter. Wolfe et al. [1980] have reported that the upstream solar wind dynamic pressure was as much as 7 to 8 times as high as its normal value during the period just before the inbound encounter with the magnetosphere. They attribute the second inbound bow shock crossing to a temporary increase in solar wind dynamic pressure, which apparently pushed the bow shock back past Pioneer 11, leaving it again in the solar wind until it re-encountered the bow shock some 5 hours later, more than 15% closer to the planet. By the time Pioneer 11 exited from the magnetosphere on the dawnside 3 1/2 days later, the solar wind dynamic pressure had diminished to near or slightly below normal. Thus, there is good evidence that the size of Saturn's magnetosphere was probably

varying considerably during the Pioneer 11 encounter. Such variations in the magnetospheric field are known to result in redistribution and energization of trapped particles [see, e.g., Brewer et al., 1969]. Thus, we should not be surprised that the steady-state assumption results in improbable convection velocities.

Granting that temporal changes were occurring during the period under consideration, we no longer can estimate point-by-point the $\vec{E} \times \vec{B}$ velocity on the basis of Pioneer 11 observations. We can, however, ask whether or not the assumption of corotation leads to unreasonable values for the temporal changes that are probably occurring. Referring to Figure 7, we see that there are several intervals of time during which the derived partial time derivative of the intensity is persistently either positive or negative. Integrating $\partial(\log M)/\partial t$ over such an interval tells us the total temporal change in M during that period. For example, the interval of persistently negative partial time derivative from 0545 to 0730 represents a net decrease in the intensity by a factor of only about 0.46, and the interval of persistently positive partial time derivative from 1000 to 1115 represents a net increase in M by a factor of 1.7. Thus, the temporal changes deduced from the assumption of exact corotation are always less than a factor of 2 one way or the other, and as we noted earlier, the net change over the entire period we have studied here is zero. On the other hand, the assumption of zero corotation leads to persistently negative time

derivatives throughout the entire interval and a net decrease in the overall intensity by almost three orders of magnitude. Such a large change seems highly improbable even in light of the very disturbed interplanetary conditions.

The error bars shown on the data points in Figures 6-8 have been computed by propagating the errors in the K_i and Δ_i through Equation (4), assuming the errors in the K_i and Δ_i are independent. We have also tested the sensitivity of our results to the adopted value of the spectral index by performing the calculations for a spectral index equal to the nominal value ± 0.5. Such a variation in γ results in derived azimuthal velocities which vary by less than about 15% from those shown in Figure 6 and which lie within the error bars shown in that figure. Thus, although uncertainties of that magnitude in the spectral index might slightly affect our quantitative results, our basic conclusions would not be significantly affected.

In summary, although these data by themselves do not allow an unambiguous determination of the extent of corotation in Saturn's outer magnetosphere, they are consistent with exact corotation at the nominal rotation period in the presence of significant but not unreasonable temporal variations in the proton population. Such a picture is supported by data from the plasma analyzer on Pioneer 11 which, as reported by Wolfe et al. [1980] and Frank et al. [this issue], found plasma flow in Saturn's magnetosphere which appears to be consistent with corotation.

Acknowledgments

We would like to thank Dr. F. B. McDonald and Dr. J. H. Trainor for the use of the GSFC/UNH data. We also thank E. J. Smith for the use of the magnetic field data. The Iowa portion of this research was supported by the National Aeronautics and Space Administration under contract NAS2-6553 and by the U. S. Office of Naval Research.

REFERENCES

Brewer, H. R., M. Schulz, and A. Eviatar, Origin of drift-periodic echoes in outer-zone electron flux, J. Geophys. Res., 74, 159, 1969.

Frank, L. A., B. G. Burek, K. L. Ackerson, J. H. Wolfe, and J. D. Mihalov, Plasmas in Saturn's magnetosphere, J. Geophys. Res., 85, this issue, 1980.

Kaiser, M. L., M. D. Desch, J. W. Warwick, and J. B. Pearce, Voyager detection of nonthermal radio emission from Saturn, submitted to Science, 1980.

McDonald, F. B., A. W. Schardt, and J. H. Trainor, If you have seen one planetary magnetosphere you haven't seen them all -- energetic particle observations in the Saturn magnetosphere, J. Geophys. Res., 85, this issue, 1980.

Northrop, T. G., and M. F. Thomsen, Theory of scan plane flux anisotropies, J. Geophys. Res., 85, this issue, 1980.

Trainor, J. H., F. B. McDonald, B. J. Teegarden, W. R. Webber, and E. C. Roelof, Energetic particles in the Jovian magnetosphere, J. Geophys. Res., 79, 3600, 1974.

Van Allen, J. A., M. F. Thomsen, B. A. Randall, R. L. Rairden, and C. L. Grosskreutz, Saturn's magnetosphere, rings, and inner satellites, Science, 207, 415, 1980a.

Van Allen, J. A., B. A. Randall, and M. F. Thomsen, Sources and sinks of energetic electrons and protons in Saturn's magnetosphere, J. Geophys. Res., 85, this issue, 1980b.

Wolfe, J. H., J. D. Mihalov, H. R. Collard, D. D. McKibbin, L. A. Frank, and D. S. Intriligator, Preliminary results on the plasma environment of Saturn from the Pioneer 11 plasma analyzer experiment, Science, 207, 403, 1980.

FIGURE CAPTIONS

Figure 1. Equatorial plane projection of the encounter trajectory of Pioneer 11 at Saturn. The spacecraft spin axis points continuously at Earth, and the detectors' look direction is perpendicular to the spin axis.

Figure 2. Fourier coefficients and phase angles from fits to 15-minute intervals of data from the University of Iowa detector G during the inbound portion of the Pioneer encounter with Saturn. Error bars are calculated from the RMS deviation between the fit and the data.

Figure 3. Comparisons between 15-minute intervals of data and the corresponding Fourier fits as described in the text. Representative error bars show the statistical uncertainty in the individual points.

Figure 4. Sample fits to the proton energy spectrum. (Left) Adopted spectral form is the sum of two power laws. (Right) Adopted spectral form is a single power law.

Figure 5. Effective power law differential spectral index at E_p = 0.61 MeV. Values at times between plotted points are obtained by linear interpolation.

Figure 6. Azimuthal component of the $\vec{E} \times \vec{B}$ convection velocity deduced from Equation (4) for a time-stationary magnetospheric configuration. The points have been smoothed by a running four-point average. The error bars are thus approximately half the size of the estimated errors in the original unsmoothed 15-minute results. Errors have been estimated by propagating the errors in the K_i and Δ_i through Equation (4), assuming the errors in the K_i and Δ_i are independent. Also shown is the azimuthal component of the convection velocity one would expect for corotation with a period of $10^h\ 40^m$ (solid line) and the least-squares fit to the data points (dashed line), which corresponds to a period of $10^h\ 6^m$.

Figure 7. Partial time derivative of the logarithm of the proton intensity deduced from Equation (4) for a magnetosphere which corotates with a period of $10^h\ 40^m$. The points have been smoothed by a running four-point average, and the comments in Figure 6 regarding the error estimates are applicable here as well.

Figure 8. Same as Figure 7 except the magnetosphere is assumed not to be corotating at all, i.e., $\vec{u}_E = 0$.

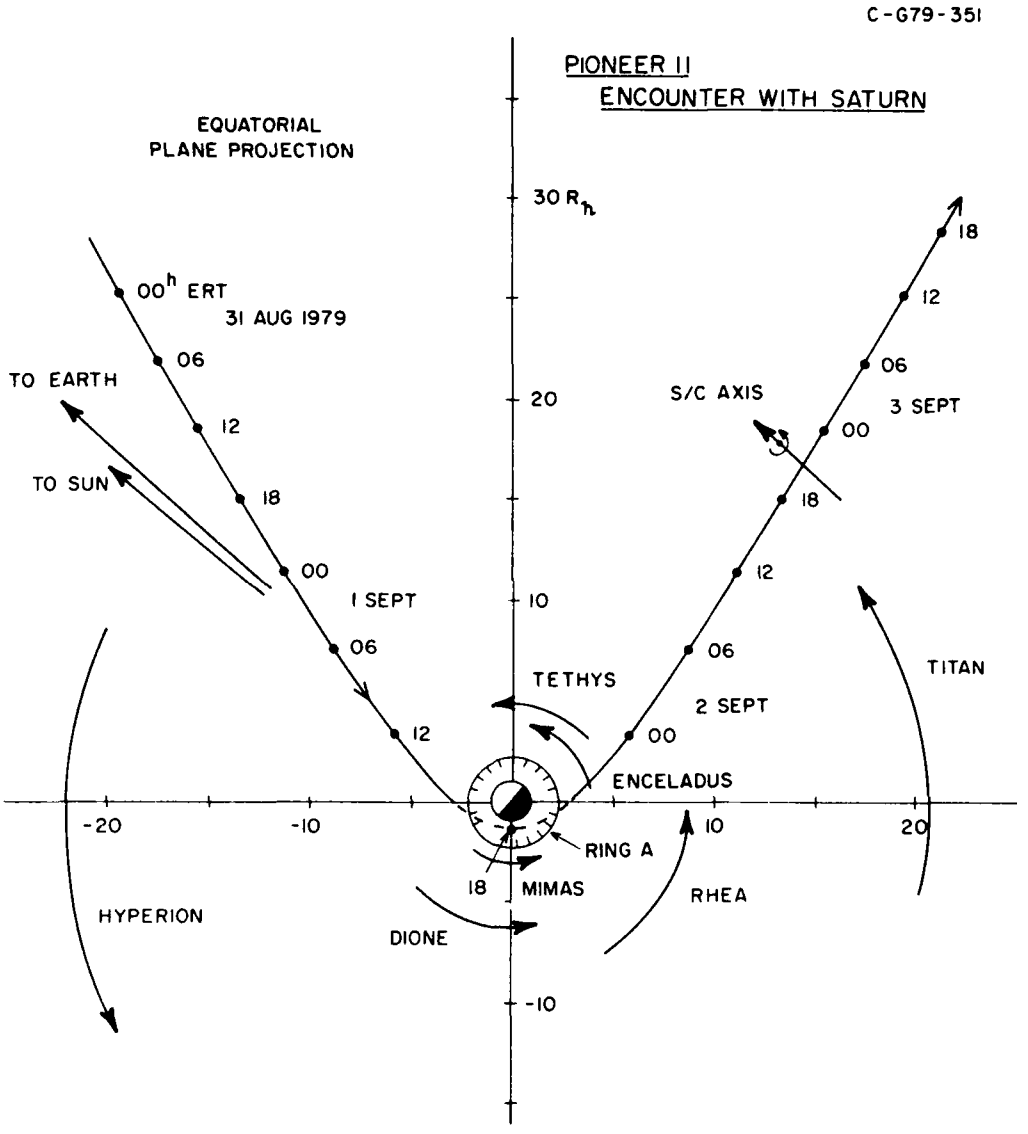
C-G79-351
PIONEER 11
ENCOUNTER WITH SATURN
EQUATORIAL
PLANE PROJECTION
30 R_h
20
10
-10
-20
-10
10
20
00h ERT
31 AUG 1979
06
12
18
00
1 SEPT
06
12
TO EARTH
TO SUN
S/C AXIS
18
00
3 SEPT
06
12
18
00
2 SEPT
06
TETHYS
ENCELADUS
RING A
MIMAS
18
TITAN
RHEA
HYPERION
DIONE

Figure 1

D-G80-261

UNIVERSITY OF IOWA PIONEER 11 DETECTOR G
15 MINUTE FITS TO
$R = M\,[1 + K_1 \cos(\phi - \Delta_1) + K_2 \cos 2(\phi - \Delta_2) + K_3 \cos 3(\phi - \Delta_3)]$

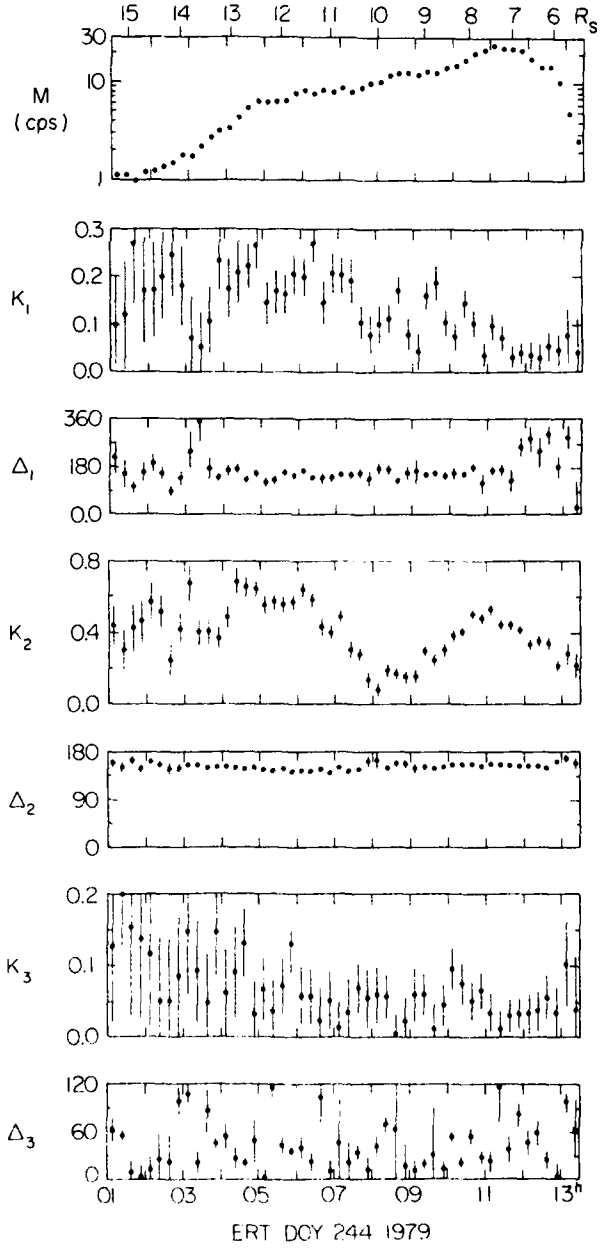

Figure 2

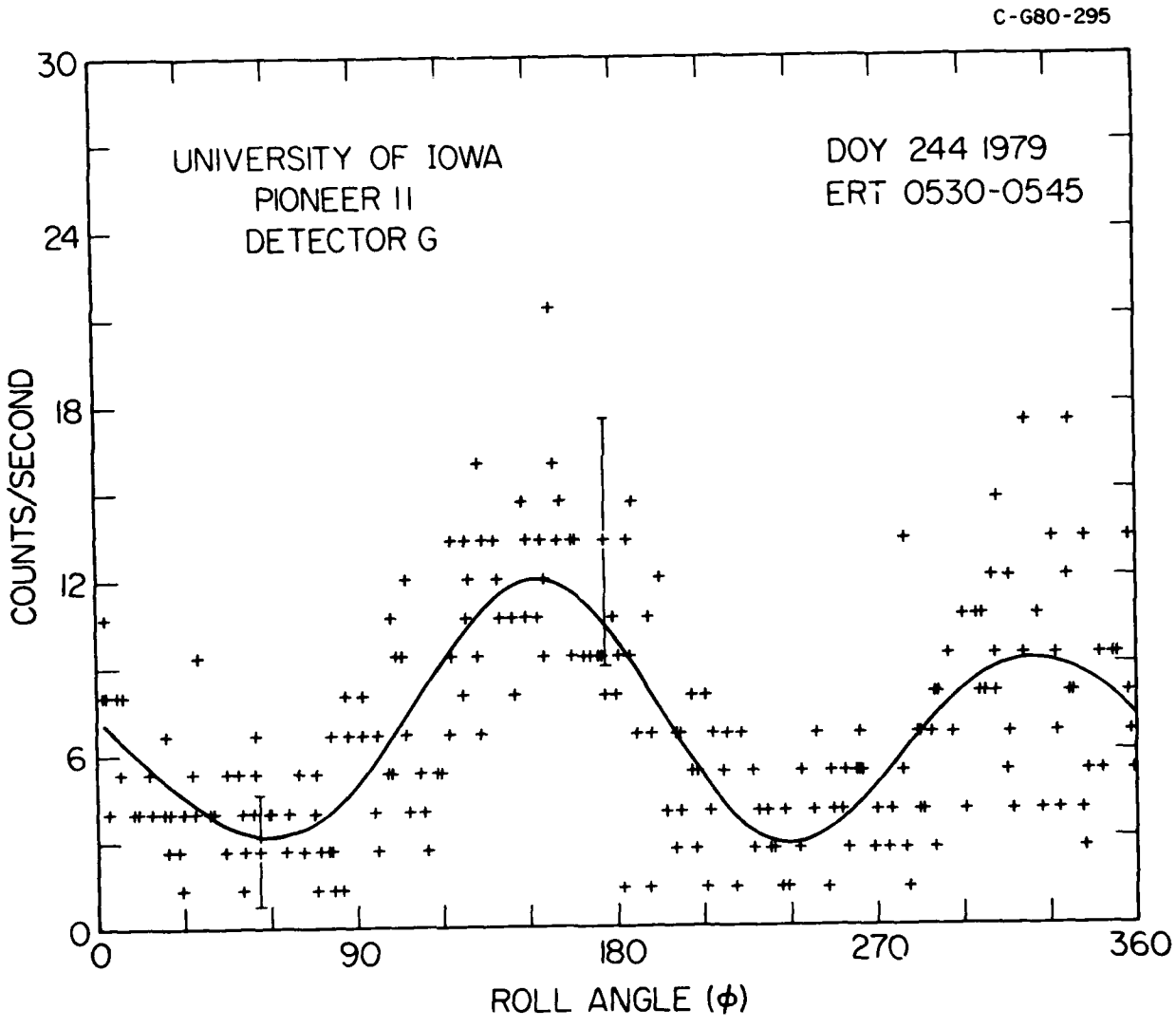
C-G80-295
UNIVERSITY OF IOWA
PIONEER II
DETECTOR G
DOY 244 1979
ERT 0530-0545
COUNTS/SECOND
ROLL ANGLE (φ)
0
6
12
18
24
30
0
90
180
270
360

Figure 3(a)

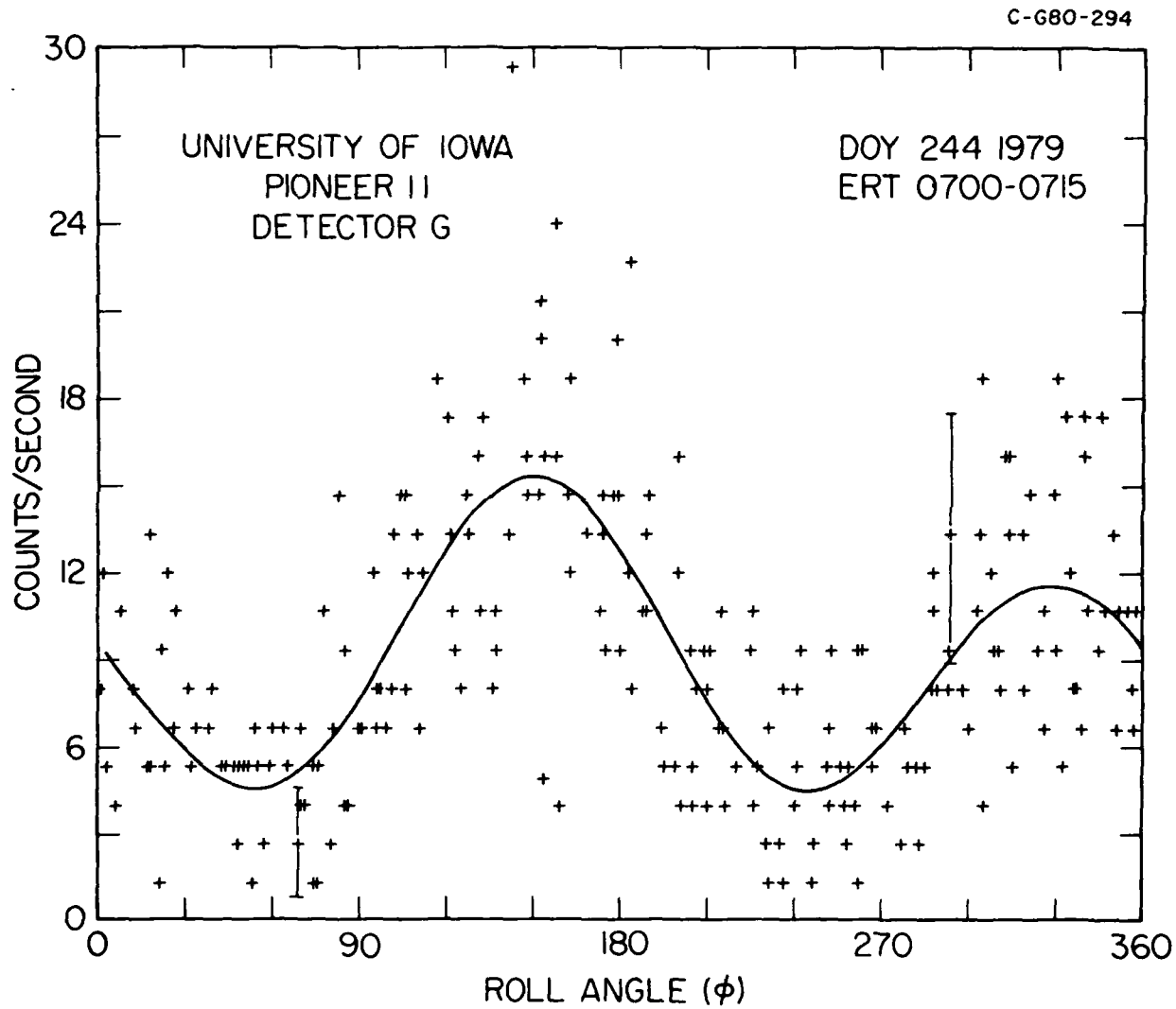
C-G80-294
UNIVERSITY OF IOWA
PIONEER 11
DETECTOR G
DOY 244 1979
ERT 0700-0715
COUNTS/SECOND
ROLL ANGLE (φ)
0
6
12
18
24
30
0
90
180
270
360

Figure 3(b)

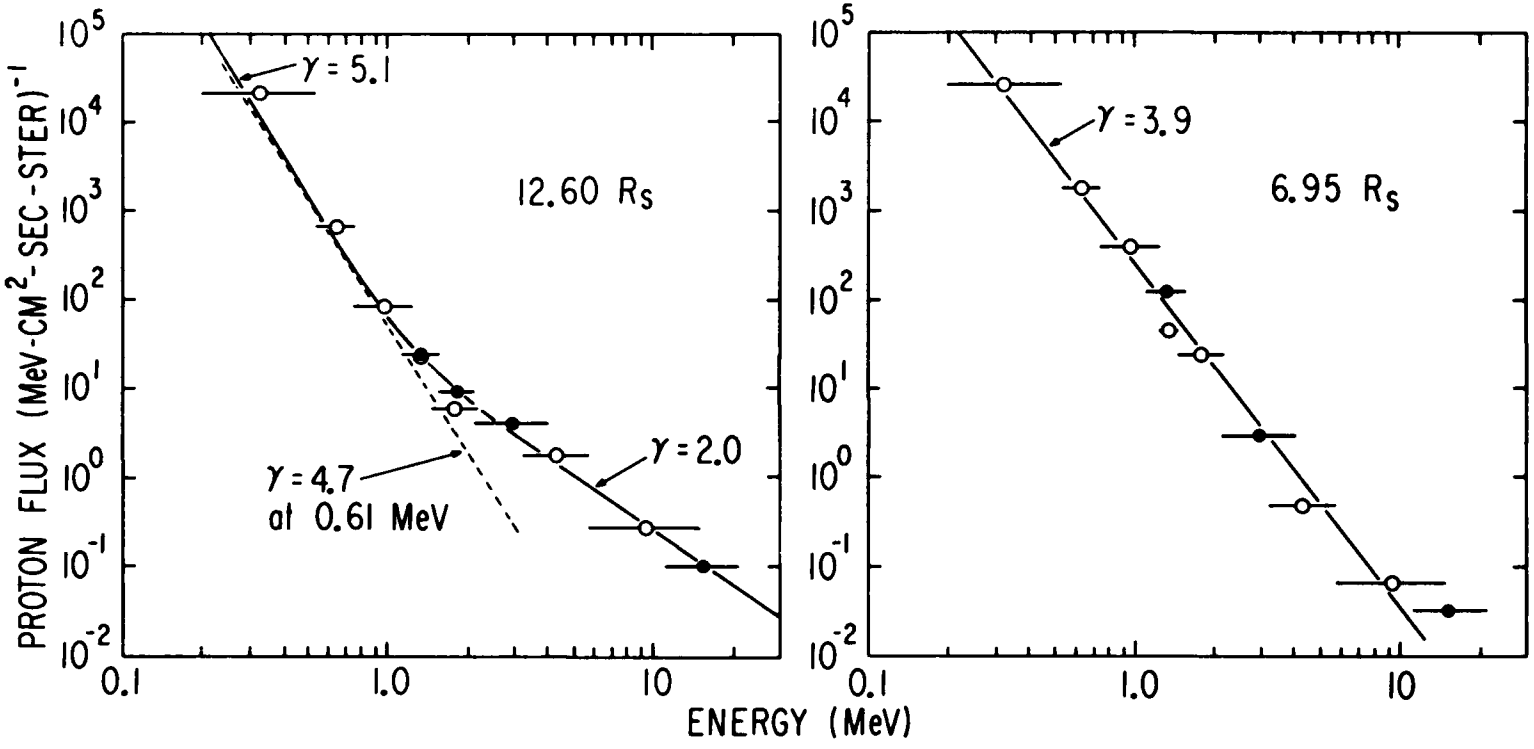
PROTON FLUX (MeV-CM^2-SEC-STER)$^{-1}$
10^5
10^4
10^3
10^2
10^1
10^0
10^{-1}
10^{-2}
$\gamma = 5.1$
12.60 R_S
$\gamma = 4.7$
at 0.61 MeV
$\gamma = 2.0$
$\gamma = 3.9$
6.95 R_S
0.1
1.0
10
ENERGY (MeV)

Figure 4

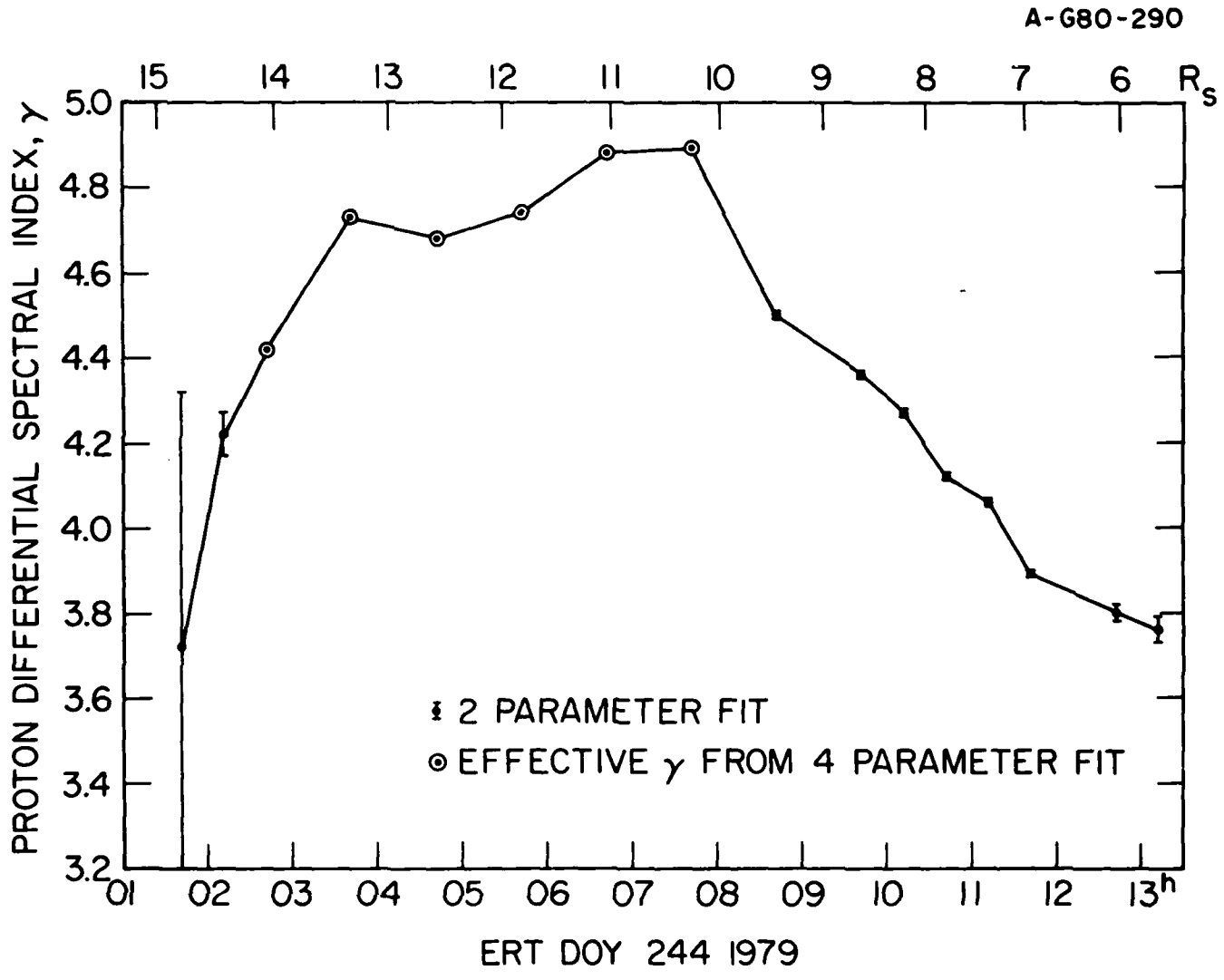
A-G80-290
15
14
13
12
11
10
9
8
7
6
R_S
PROTON DIFFERENTIAL SPECTRAL INDEX, γ
5.0
4.8
4.6
4.4
4.2
4.0
3.8
3.6
3.4
3.2
2 PARAMETER FIT
EFFECTIVE γ FROM 4 PARAMETER FIT
01
02
03
04
05
06
07
08
09
10
11
12
13h
ERT DOY 244 1979

Figure 5

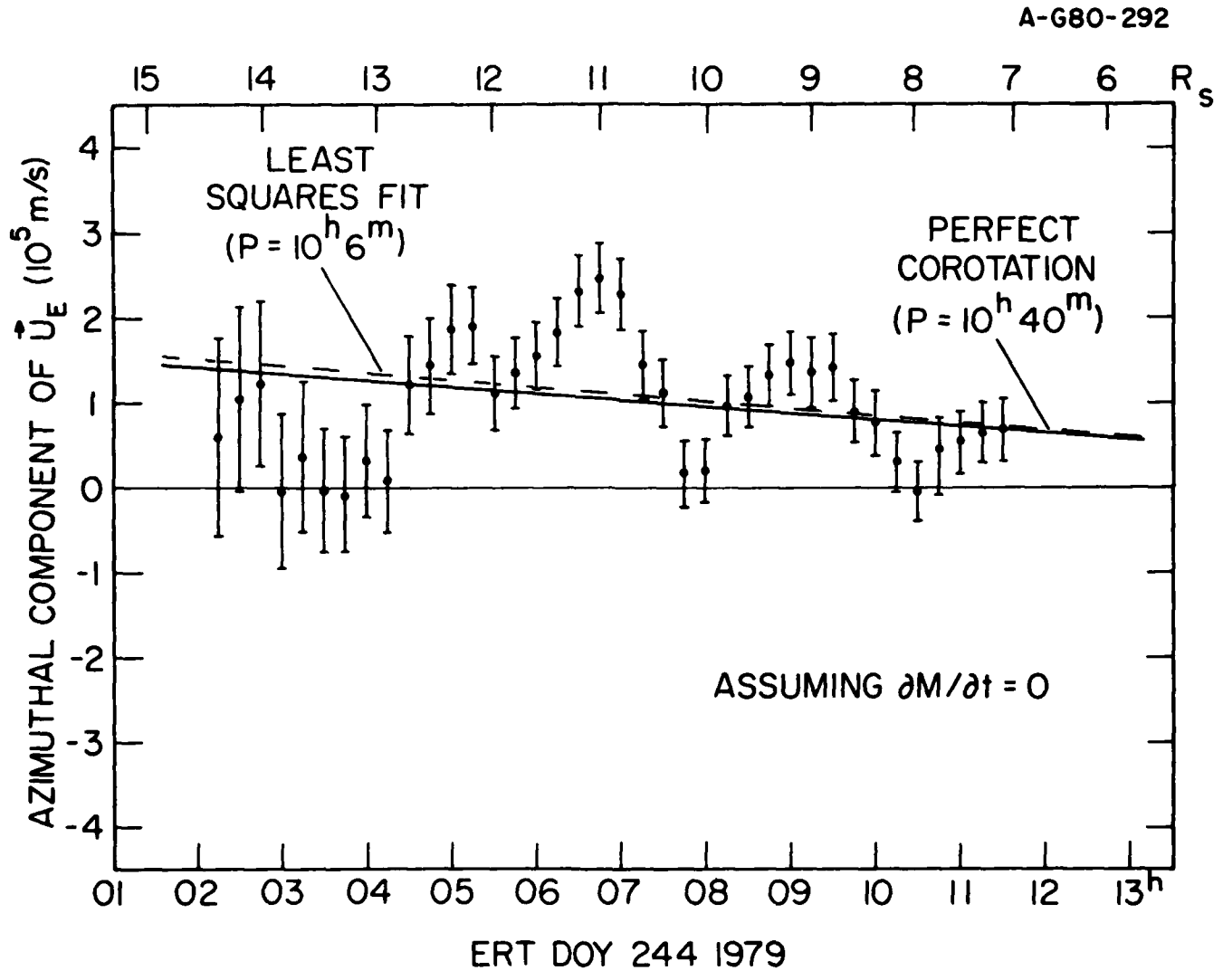
A-G80-292
15
14
13
12
11
10
9
8
7
6
R_S
LEAST
SQUARES FIT
($P = 10^h 6^m$)
PERFECT
COROTATION
($P = 10^h 40^m$)
ASSUMING $\partial M/\partial t = 0$
AZIMUTHAL COMPONENT OF $\hat{U}_E$ (10^5 m/s)
4
3
2
1
0
-1
-2
-3
-4
01
02
03
04
05
06
07
08
09
10
11
12
13^h
ERT DOY 244 1979

Figure 6

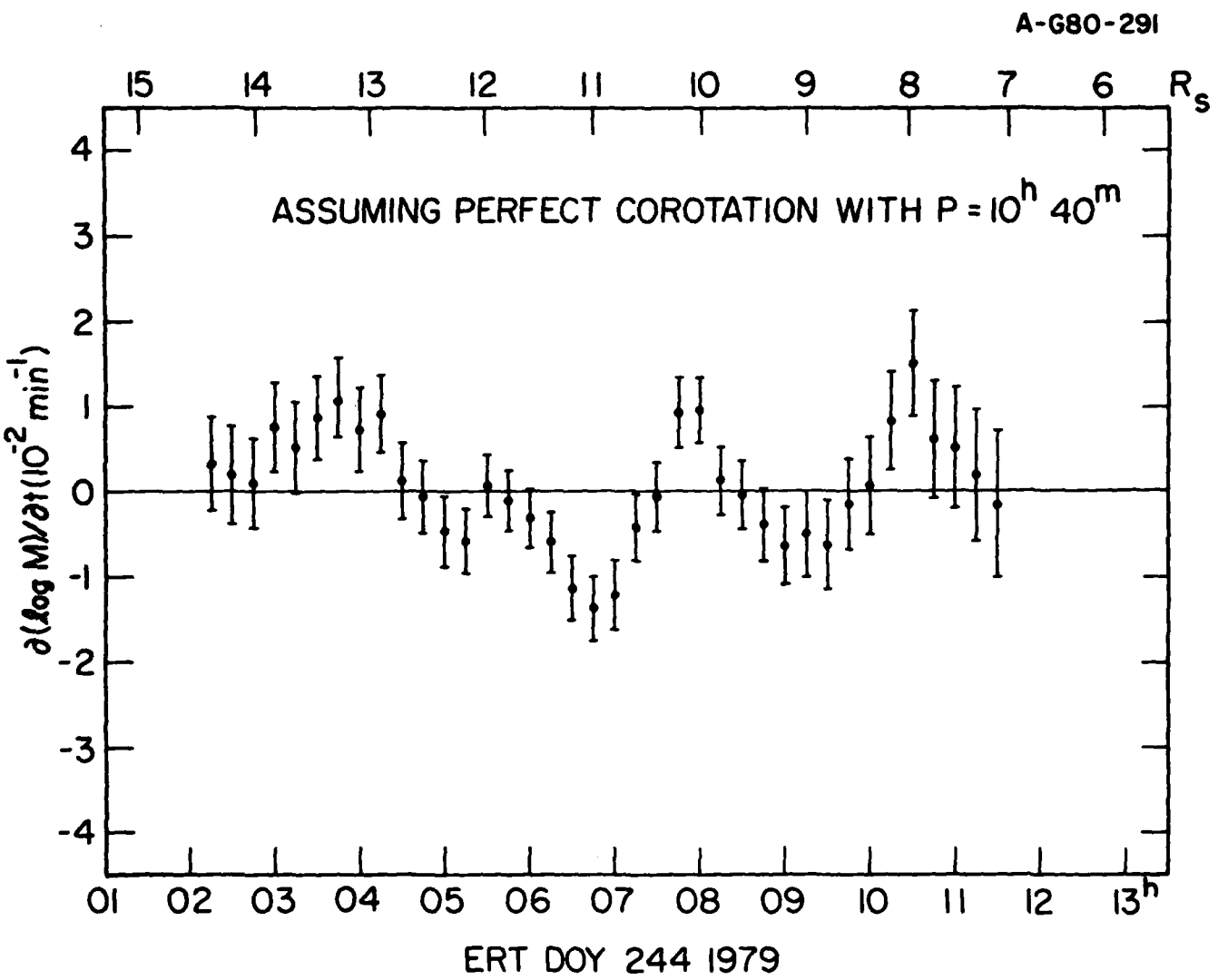
A-G80-291
15
14
13
12
11
10
9
8
7
6
R_S
ASSUMING PERFECT COROTATION WITH P = 10^h 40^m
$\partial(\text{Log } M)/\partial t\,(10^{-2}\,\text{min}^{-1})$
4
3
2
1
0
-1
-2
-3
-4
01
02
03
04
05
06
07
08
09
10
11
12
13^h
ERT DOY 244 1979

Figure 7

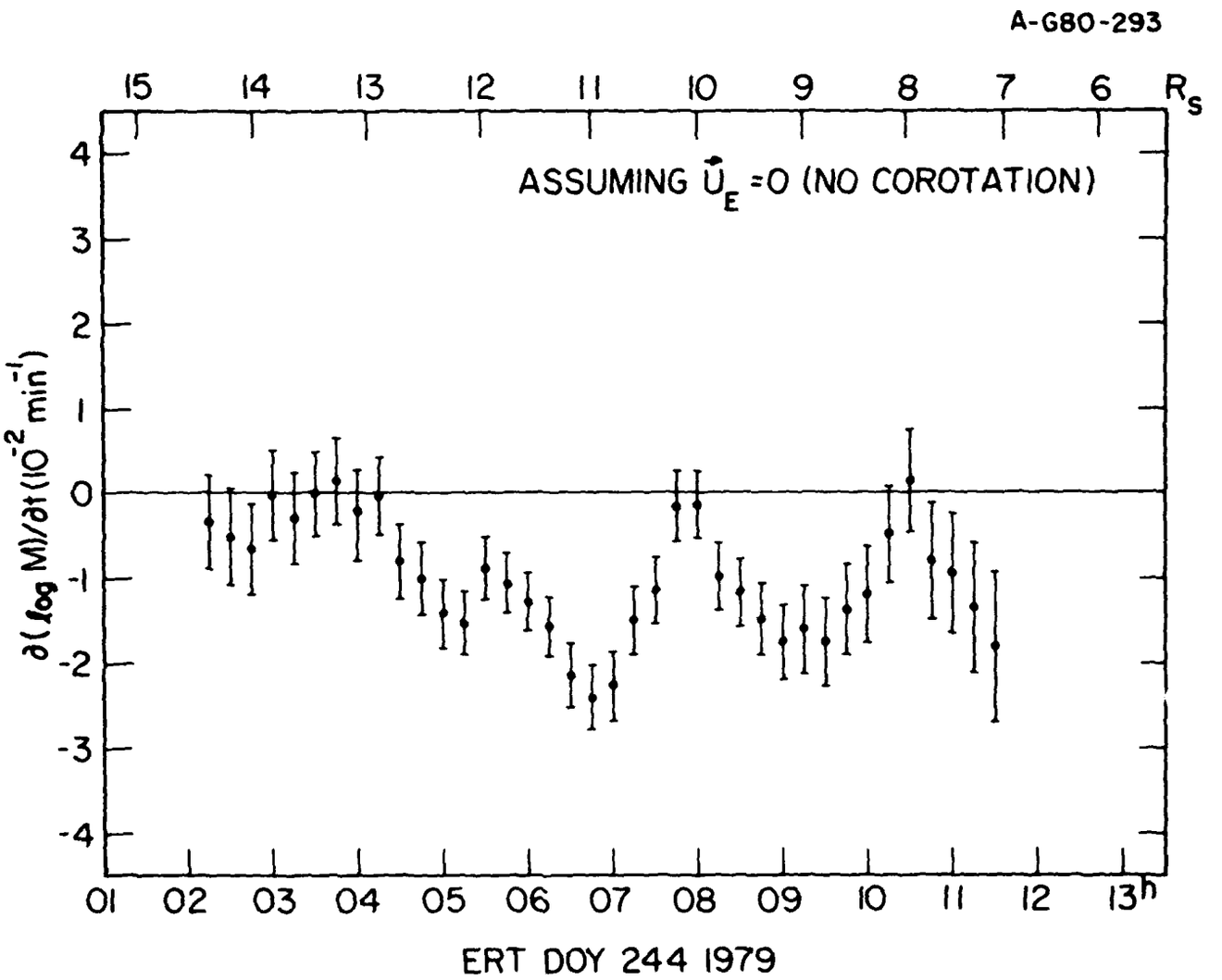
A-G80-293
15 14 13 12 11 10 9 8 7 6 R_S
ASSUMING $\vec{U}_E$ =0 (NO COROTATION)
4 3 2 1 0 -1 -2 -3 -4
$\partial(\log M)/\partial t (10^{-2}\ min^{-1})$
01 02 03 04 05 06 07 08 09 10 11 12 13h
ERT DOY 244 1979

Figure 8